Magnetorheology of fiber suspensions. II. Theory

Pavel Kuzhir, Modesto Lopez-Lopez, Georges Bossis

TITLE OF THE ARTICLE:

Magnetorheology of fiber suspensions. II. Theory

AUTHORS:

Pavel Kuzhir, Modesto T. López-López,[1] Georges Bossis

Laboratoire de Physique de la Matière Condensée, CNRS UMR 6622 Université de Nice, Parc Valrose, 06108 Nice Cedex 2, France

[1] Present address: Department of Applied Physics, University of Granada, Avda. Fuentenueva s/n, 18017 Granada, Spain.

CORRESPONDING AUTHOR:

Pavel Kuzhir. E-mail: kuzhir@unice.fr

SYNOPSIS

This paper reports the first predictions of the yield stress of suspensions of non-Brownian magnetic fibers in the presence of uniform magnetic fields. The quasi-static regime of the shear deformation (before the flow onset) of the suspension is studied. Four different structures of the magnetic fiber suspensions are considered – column, zigzag, 3D stochastic and near-planar stochastic structures – and the yield stress is attributed to the failure of the given structure at a critical strain. The main contributions to the yield stress are found to come from the restoring magnetic torque acting on each fiber and from the solid friction between fibers. The enhanced magnetorheological effect of magnetic fiber suspensions observed experimentally (companion paper) is explained and quantified in terms of interfiber friction. Surprisingly, the dipolar magnetic interactions between fibers do not affect significantly the yield stress. The lowest yield stress is obtained for the zigzag structure and the highest one for the column structure. A reasonable agreement with the experiments is obtained for 5 and 7 %

fiber volume fractions in the frame of the more realistic model of near-planar stochastic structures.

I. INTRODUCTION

The theoretical study of nonmagnetic fiber suspensions started with the work of Jeffery (1922) who calculated the rotation of a single elongated particle in shear flow. Jeffery's results were subsequently used for the calculation of the stress tensor of diluted fiber suspensions [Batchelor (1970); Brenner (1974); Hinch and Leal (1973)], as well as of semi-diluted and concentrated suspensions with either long-range or short-range hydrodynamic interactions [Batchelor (1971); Shaqfeh and Fredrickson (1990); Doi and Edwards (1986); Folgar and Tucker (1984); Joung et al. (2001); Powell (1990); Qi (2006); Rahnama et al. (1995); Yamamoto and Matsuoka (1995)]. Useful reviews are given by Ganani and Powell (1985), Larson (1999), Petrie (1999) and Zirnsak et al. (1994).

Unfortunately, the predictions of the theories that take into account only hydrodynamic interactions, fail for rather concentrated fiber suspensions. In this case, the contact forces between fibers give a significant contribution to the stress. In concentrated suspensions, the fibers create an entangled elastic network and experience solid friction when sliding over each other [Petrich and Koch (1998)]. Such suspensions possess a yield stress attributed to the interfiber failure of the network. Bennington et al. (1990) reported the first attempt to include the interparticle friction in order to calculate the yield stress in fiber suspensions. A more rigorous model that takes into account stochastic fiber orientations was reported by Toll and Manson (1994) for planar fiber suspensions. This theory gives a reasonably good prediction of the yield stress of planar fiber suspensions measured in shear and squeeze flow [Servais et al. (1999); (2002)]. A more general theory for real 3D fiber suspensions has recently been reported [Djalili-Moghaddam and Toll (2005)]. This theory

incorporates both long-range hydrodynamic interactions and short-range interactions (near the contact point between two fibers) and gives a reasonably good correspondence with experimental results for the viscosity of fiber suspensions.

Particle level dynamic simulations of sheared flexible fiber suspensions have also been performed and have shown the extreme importance of the interfiber friction coefficient in the flocculation and rheology of the suspensions [Schmid et al. (2000); Schmid and Klingenberg (2000); Switzer and Klingenberg (2004); Lindstrom and Uesaka (2007)].

Note that colloidal forces between particles can also give rise to a significant yield stress in fiber suspensions [Philipse and Wierenga (1998); Wierenga et al. (1998); Hovarth and Lindstrom (2007)]. However, colloidal interactions are significant for submicron particles and are expected to play a minor role for the relatively large fibers used in our experiments. The other interaction that could provoke a gelation of a fiber suspension is the magnetic interaction. In suspensions of spherical magnetic particles, the application of a magnetic field causes the formation of a network of particles or aggregates throughout the suspension, which gives rise to the appearance of large yield stresses –up to 100 kPa [Bossis et al. (2002); Ginder (1998)]. This phenomenon is known as magnetorheological effect and these suspensions are called magnetorheological (MR) suspensions. The rheology of conventional MR suspensions (suspensions of spherical magnetic particles) has been widely investigated since the first study reported by Winslow (1949). Detailed reviews can be found in Bossis et al. (2002), Ginder (1998), Larson (1999), Shulman (1996) and Shulman and Kordonsky (1982).

Whereas the rheology of suspensions of either nonmagnetic fibers or magnetic spherical particles has been the subject of thousands of papers and a few monographs, too little attention has been paid to the rheology of suspensions of magnetic fibers, especially non-Brownian ones. Nevertheless, due to the shape anisotropy of fibers and the possible existence

of friction between them, their use in MR suspensions could enhance significantly the MR effect [López-López et al. (2007)]. Furthermore, an interesting rheological behavior is expected for such magnetic fiber suspensions, combining the behaviors observed in nonmagnetic fiber suspensions and in conventional MR suspensions. Some experimental rheological data on the rheology of elongated particle suspensions that support this statement are reported in the papers by López-López et al. (2007), Kuzhir et al. (2007), Bell et al. (2008) and Ngatu et al. (2008). A detailed experimental investigation on the shear rheology of magnetic fiber suspensions, including the concentration dependence of the yield stress and observations of the suspension structures under applied magnetic field, is presented in the companion paper. A two- to three-time increase in the yield stress of magnetic fiber suspensions compared to suspensions of spherical magnetic particles was found. However, no theoretical model explaining this increase has been reported. In the present paper, we introduce the first microstructural models for magnetic fiber suspensions and explain the enhanced magnetorheological response of these suspensions in terms of interfiber solid friction. Our theory covers the quasi-static regime of the shear deformation (before the flow onset) and combines the features of the point-wise interaction theory developed by Toll and Manson (1994) for classical fiber suspensions and the features of the column structure and zigzag structure models for classical MR suspensions [Bossis et al. (1997); Volkova (1998)].

In contrast to suspensions of non-Brownian magnetic fibers, colloidal dispersions of nano-sized elongated magnetic particles have been studied theoretically in some detail [Aoshima and Satoh (2008); Rubí et al. (1993); Salueña et al. (1994); Satoh (2001, 2003, 2005), Tsebers (1984)]. These authors predicted for these dispersions an increase in viscosity and a shear thinning behavior upon magnetic field application, but no field-induced yield stress due to the intense Brownian motion. This behavior was confirmed experimentally [Maiorov (1980)].

The present paper is outlined as follows. In the following section we consider the different interactions in magnetic fiber suspensions and we compare their energies. This allows us to determine the dominating interactions and, subsequently, to exclude the less important ones from our theory. In section III, we construct a micromechanical model for four particular structures of the magnetic fiber suspensions: (i) column structures; (ii) zigzag structures; and more realistic (iii) 3D stochastic structures and (iv) near-planar stochastic structures. Finally, in section IV all these models are tested by comparing their predictions with the experimental results reported in the companion paper.

II. INTERACTIONS IN FIBER SUSPENSION

When a suspension of non-Brownian magnetic fibers is subjected to a magnetic field, the fibers get magnetized, are attracted to each other and form an entangled network, as described in the companion paper. The suspension yield stress is directly affected by the mechanical strength of the fiber network, which, in turn, depends on the interfiber interactions. In our analysis, we shall consider only very long (or very thin) magnetic fibers, with aspect ratio $l/d \geq 10$. In the presence of magnetic field, we expect at least the following interactions in suspensions of long fibers:

a) Interaction between the fibers and the field. The magnetic field exerts a magnetic torque on a fiber, which tends to align it with the field. The energy of this interaction scales as

$$U_m \propto mH = \mu_0 M V_f H\,, \tag{1}$$

where $m = \mu_0 M V_f$ is the magnetic moment of the fiber, H the magnetic field intensity in A/m, M the magnetization of the fiber material in A/m, $V_f = \pi d^2 l/4$ the volume of the fiber, d and l

the fiber diameter and length respectively, and $\mu_0 = 4\pi\ 10^{-7}$ Henry/m the magnetic permeability of vacuum.

b) Magnetic interaction between fibers. Let us assume that fibers are dipoles with the north and the south poles situated on the fibers extremities. The total interaction is therefore the sum of the pair interactions between the poles of the fibers. The characteristic energy of such interaction is

$$U_d \propto \frac{p^2}{4\pi\mu_0 r} \propto \mu_0 M^2 V_f \frac{d^2}{lr}. \qquad (2)$$

In this formula $p = m/l$ is the intensity of the "magnetic poles" and r is the distance between the poles of neighboring fibers.

c) Mechanical contacts between fibers. They are manifested through a normal reaction force, f_n, and a tangential friction force, which is assumed to be Columbic: $f_\tau = \xi f_n$, with ξ being the friction coefficient. Under shear deformation, the fibers slip along each other and the energy dissipated per fiber is equal to the work of the friction forces acting on a given fiber: $W_{fr} \propto \xi f_n \Delta x$, with $\Delta x \sim l$ being the displacement of one fiber relative to another one. When the fibers are misaligned with the magnetic field, the normal contact forces equilibrate the magnetic torque, $T_m \propto mH$, acting on the fiber, and therefore $f_n \propto \frac{T_m}{l} = \frac{\mu_0 M V_f H}{l}$. Finally, the expression for the work W_{fr} takes the form

$$W_{fr} \propto \xi \mu_0 M V_f H. \qquad (3)$$

Let us now compare the interaction energies. Dividing equation (2) by equation (1), we get the ratio between the dipolar interaction energy and the "fiber-field" interaction energy:

$$\frac{U_d}{U_m} \propto \frac{M d^2}{H l r} \ . \qquad (4)$$

According to the experimental observations, the fibers in the suspension can touch each other either by their extremities or by their lateral cylindrical surfaces (see Figure 8 of the companion paper). In the former case, the distance between the poles of neighboring fibers, *r*, is of the order of the fiber diameter, *d*, and the energy ratio (4) scales as $\frac{U_d}{U_m} \propto \frac{Md}{Hl}$. In the latter case, the contact point is located somewhere between the fiber extremities, and for long fibers the distance *r* is of the order of the fiber length, *l*, and the energy ratio (4) becomes $\frac{U_d}{U_m} \propto \frac{M}{H}\left(\frac{d}{l}\right)^2$. We estimated the energy ratio (4) for both cases, at low and high magnetic field and for a fiber aspect ratio $l/d \sim 10$. These estimations are summarized in Table 1. From data in Table 1, the dipolar magnetic interaction seems to be weaker than the "fiber-field" interaction, except for end-by-end alignment of fibers at low magnetic field.

Table 1. Comparison between dipolar "fiber-fiber" and "fiber-field" interactions.

	End-by-end contact		Side-by-side contact	
	Low field $0 < H \le 50$ kA/m	High field $H \ge 200$ kA/m	Low field $0 < H \le 50$ kA/m	High field $H \ge 200$ kA/m
Fiber magnetization	$M = \chi H \sim (10 \div 10^2)H$	$M \sim H$	$M = \chi H \sim (10 \div 10^2)H$	$M \sim H$
Energy ratio (equation 6)	$\frac{U_d}{U_m} \propto \frac{Md}{Hl} \propto \chi \frac{d}{l}$	$\frac{U_d}{U_m} \propto \frac{d}{l}$	$\frac{U_d}{U_m} \propto \frac{M}{H}\left(\frac{d}{l}\right)^2 \propto \chi\left(\frac{d}{l}\right)^2$	$\frac{U_d}{U_m} \propto \left(\frac{d}{l}\right)^2$
Energy ratio (numerical value)	$\frac{U_d}{U_m} \propto 1 \div 10$	$\frac{U_d}{U_m} \propto 0.1$	$\frac{U_d}{U_m} \propto 0.1 \div 1$	$\frac{U_d}{U_m} \propto 0.01$

Dividing equation (3) by equation (1), we get the ratio between the energy dissipated by solid friction and the "fiber-field" magnetic interaction energy: $W_{fr}/U_m \propto \xi$. Petrich and Koch (1998) reported a value $\xi \sim 0.4$ for the friction coefficient of polymeric fibers. We do

not have the value of the friction coefficient for our cobalt fibers, but it should be much larger than the value for polymeric fibers due to the high roughness of the fiber surface [Lopez-Lopez et al. (2007)]. Thus, the work of the friction force should be at least of the same order of magnitude than the magnetic energy, U_m. Therefore, we expect an important contribution of the friction forces to the yield stress.

Finally, note that colloidal forces and Brownian motion are not considered because the corresponding characteristic energies are much lower than the energy of the magnetic interaction: $U_{VdW}/U_m \propto A_H/(\mu_0 MH \cdot hdl) \sim 10^{-5}$ and $U_{Br}/U_m \propto kT/(\mu_0 MH \cdot d^2 l) \sim 10^{-10}$, U_{VdW} and U_{Br} being respectively the characteristic energies of the van der Waals interaction and the Brownian motion. Here $A_H \sim 10^{-19}$ is the Hamaker constant, $h \sim 4$ nm is twice the typical thickness of the layer of surfactant grafted on the particles [Lopez-Lopez et al. (2008)]. The fiber diameter and length were taken $d \sim 5$ μm and $l \sim 50$ μm, respectively. Note that the hydrodynamic interactions are also neglected because the quasi-static deformation of the suspensions without any flow is considered.

The three above considered interactions –"fiber-field", dipolar "fiber-fiber" and solid friction between fibers– will now be incorporated into the theoretical model in order to predict the yield stress of a fiber suspension in the presence of magnetic field. The shear stress of the structured suspension will be calculated for the quasi-static deformation of its structure (before the flow onset) as the sum of the particle stresses. Consequently, we need to know the arrangement of fibers in the suspension structure. Four different structures will be considered in this paper. We shall start with the simplest model of the column structure, which possesses the highest possible anisotropy, and is usually observed in conventional MR suspensions, composed of spherical magnetic particles [Bossis et al. (1997); Zubarev and Iskakova (2006)].

III. MICROSTRUCTURAL MODELS

III.1. COLUMN STRUCTURE

Let us consider a suspension of identical magnetic fibers confined between two infinite plates. The distance between these plates is supposed to be much larger than the fiber length. When the magnetic field is applied normally to the plates, the fibers gather into straight columns aligned with the field direction and spanning the gap between the plates, like shown in Figure 1a. The suspension is sheared by a displacement of the upper plate, and the strain angle is Θ. In this model, we consider that in each column the fibers overlap each other at the same overlap length, b_0 (Figure 2a). When the suspension is strained, the fibers slip along each other and the columns extend and tilt. If the fibers in the columns do not slip on the plates, each column is tilted at the angle Θ under shear (Figure 1b). Such regular network resists the shear deformation. There are at least three mechanisms of fiber suspension response to the applied strain. First, each fiber experiences a restoring magnetic torque that tends to turn it back to the vertical position. Second, the solid friction between fibers hinders the extension of the columns and, consequently, the overall strain deformation of the suspension. Finally, the magnetic dipolar attraction between fibers must be overcome in order to break the structure and to make the MR fluid flow. Firstly, we shall incorporate into our model the two first mechanisms.

The fibers touch each other by their lateral cylindrical surface and, therefore, their contact area is reduced to a line of length b (Figure 2c). The contact forces are assumed to be distributed homogeneously along the contact line and, therefore, they can be considered to be concentrated in a single point of the contact line – at the center of the overlapping section b. Two forces are exerted at each contact point: the normal force, f_n, and the tangential friction force, $f_\tau = \xi f_n$. The torque balance on each fiber gives:

$$T_m = f_n 2s + f_\tau d\,, \tag{5}$$

s being the distance between the central cross-section of the fiber and the contact point (Figure 1b). If the contact point is located far from the center of the long fiber (*s* >> *d*), we neglect the second term in equation (5) and the normal force is therefore:

$$f_n \approx \frac{T_m}{2s}. \tag{6}$$

The mechanical stresses arising in fiber suspensions are due to the contact forces exerted on the fibers. Since the carrier liquid is not elastic but Newtonian and there is not any significant flow in the quasi-static deformation regime, the only contribution to the suspension stress tensor is the particle stress. This is a volume average of the stresses contributed by each fiber. In our particular case, since the forces acting on the fibers are concentrated in single points (point-wise interactions), the expression for the suspension shear stress is given by [Larson (1999); Toll and Manson (1994)]:

$$\tau = \frac{1}{V}\sum_{\text{fibers}}\sum_{\text{contacts}} r_z f_y \ . \tag{7}$$

Here *V* is the total volume of the suspension, *r* is the distance between the fiber center and the contact point and the sum is taken over all the contact points on every particle of the suspension. Since we have two contact points per fiber, the expression (7) takes the form:

$$\tau = \frac{N_f}{V}\left(2r_z f_y\right) = \frac{\Phi}{V_f}\left(2r_z f_y\right). \tag{8}$$

Here N_f is the total number of fibers in the suspension volume, *V*; V_f is the fiber volume and Φ is the volume fraction of fibers. The z-component of the distance, *r*, is $r_z = s\cos\Theta + (d/2)\sin\Theta \approx s\cos\Theta$, and the y-component of the contact force, **f**, is the sum of the corresponding components of the normal and friction forces: $f_y = f_n\cos\Theta + f_\tau\sin\Theta = f_n(\cos\Theta + \xi\sin\Theta)$. Substituting these expressions into equation (8) and replacing f_n by the appropriate formula (6), we get:

$$\tau = \frac{\Phi}{V_f} T_m \left(\cos^2 \Theta + \frac{1}{2} \xi \sin 2\Theta \right) \tag{9}$$

The magnetic torque exerted on a fiber is given by the expression:

$$T_m = mH \sin\psi = \mu_0 M V_f H \sin\psi \,. \tag{10}$$

Here ψ is the angle between the vectors of the magnetic moment of the fiber, **m**, and the magnetic field intensity **H**. The magnetization of the fibers, *M*, is a function of the magnetic field intensity H_f inside the fibers: $M = \chi_f(H_f) H_f$ with χ_f being the fiber magnetic susceptibility. The field H_f (cf. equation A.5) and the angle ψ are defined in the same way as for an infinitely prolate ellipsoid subjected to an uniform magnetic field, *H*, applied at an angle Θ with respect to the major axis of the ellipsoid [Landau and Lifshitz (1960)]. Substituting the expressions for *M* and $\sin\psi$ into equation (10), we get the following formula for the magnetic torque:

$$T_m = \frac{1}{2} \mu_0 \frac{\chi_f^{\,2}}{2 + \chi_f} V_f \; H^2 \sin 2\Theta \,. \tag{11}$$

And the final expression for the shear stress reads:

$$\tau = \tau_m + \tau_{fr} = \frac{1}{2} \Phi \frac{\chi_f^{\,2}}{2 + \chi_f} \mu_0 \; H^2 \left(\sin(2\Theta) \cos^2 \Theta + \frac{1}{2} \xi \sin^2 2\Theta \right). \tag{12}$$

The first term τ_m is the contribution of the "fiber-field" interaction and the second term τ_{fr} is the contribution of the friction forces. The magnetic field, *H*, is in fact the mean magnetic field inside the MR suspension. It is related to the external magnetic field, H_0, through the relative magnetic permeability of the fiber suspension. Its calculation is summarized in the Appendix.

The stress-strain curves calculated by equation (12) are presented in Figure 3 for two values of the friction coefficient, ξ = 0 and 1, for a magnetic field H_0 = 100 kA/m, and for a volume fraction Φ = 0.05. As expected, these curves have a maximum at some critical strain

angle, Θ_c. Above this critical strain the static column structure becomes unstable (Figure 1c), breaks and the flow starts (Figure 1d). In case of small initial overlap of fibers, they can be aligned end-by-end at subcritical angles (cf. Figure 1e). Such configuration will also be unstable, and the fibers will turn towards the vertical position under the action of the magnetic torque (Figure 1g), they will detach from each other and the flow will start (Figure 1h). Consequently, the column structure breaks either at the critical angle Θ_c or at the angle $\Theta_a = a\cos(1-\beta_0)$, corresponding to the end-by-end alignment, $\beta_0 = b_0/l$ being the dimensionless overlap. The yield stress of the fiber suspension is the shear stress at which the column structure breaks; it is given by equation (12), in which we must replace the angle Θ by the yield angle, $\Theta_Y = \min[\Theta_c\ ,\ a\cos(1-\beta_0)]$, being the minimum strain angle corresponding to the structure failure.

At sufficiently large overlaps, $\beta_0 \geq 0.15$, the yield stress corresponds to the maximum of the stress-strain curve. This maximum is shifted towards larger values of Θ when the friction coefficient is increased (Figure 3), and it is determined by the condition $\frac{\partial \tau}{\partial \theta} = 0$. To get an approximate value of the angle Θ_c, we assume both χ_f and H to be independent of the strain angle, Θ, and in this way we obtain the following equation for Θ_c:

$$\cos 2\Theta_c + \cos 4\Theta_c + \xi \sin 4\Theta_c = 0 \qquad (13)$$

Such approximation gives only a 5% error on the yield stress. For a friction coefficient, $\xi = 1$, we get a critical angle, $\Theta_c \approx 37^o$. In the absence of friction, $\xi = 0$, equation (13) gives $\Theta_c \approx 30^o$, which corresponds to a yield stress:

$$\tau_Y = \frac{3\sqrt{3}}{16}\Phi\frac{{\chi_f}^2}{2+\chi_f}\mu_0 H^2 \qquad (14)$$

We shall compare these calculations with the experimental results in the last section of the present paper. Note that, in the extreme cases of very low or very high magnetic field, we can

replace the term $\frac{\chi_f^{\,2}}{2+\chi_f}\mu_0 H^2$ in equations (13) and (14) by $\chi_f \mu_0 H^2$ or $\frac{1}{2}\mu_0 M_s^{\,2}$, respectively.

We shall now include the dipolar magnetic interactions between fibers in our model. We suppose our fibers to be long sphero-cylinders with north (–) and south (+) magnetic poles, of intensity *p*, located in the center of the end hemispheres, as shown in Figure 2c. The (–)-pole of the lower fiber is attracted to the (+)-pole and repulsed by the (–)-pole of the upper fiber (forces $f_{\pm}$ and $f_{\overline{-}}$, respectively). On the other hand, the (+)-pole of the lower fiber is attracted to the (–)-pole and repulsed by the (+)-pole of the upper fiber (forces $f_{\mp}$ and $f_{\substack{+\\+}}$, respectively). The total interaction is the vector sum of these four forces. Each of these forces is equivalent to the electrostatic force acting between two electric charges: it is oriented along the line joining the centers of the interacting poles and follows Coulomb's law:

$$f_{ij} = \frac{p^2}{4\pi\mu_0 r_{ij}^2} \tag{15}$$

Here i = +,–; j = +,– and $p = \frac{m}{l}$ is the intensity of the magnetic pole of a fiber.

Since $f_{ij} \propto 1/r_{ij}^2$, the strongest dipolar interaction is reached when the extremities of the neighboring fibers are in contact. Therefore, it is reasonable to take into account only the interaction between the two closest poles of neighboring fibers. Then, including these forces in the torque balance (5) and in the stress equation (7), and performing the necessary calculations, we arrive to the final expression for the shear stress:

$$\tau = \tau_m + \tau_{fr} + \tau_d = \frac{\Phi\chi_f^{\,2}\mu_0 H^2}{2(2+\chi_f)}\left\{\sin(2\Theta)\cos^2\Theta + \frac{1}{2}\xi\sin^2 2\Theta - \frac{G}{16}\left(\frac{d}{l}\right)^2 \sin 2\Theta\left(\left(2+\chi_f\right)\cos^2\Theta + \frac{4}{2+\chi_f}\sin^2\Theta\right)\right\} \tag{16}$$

Here, $G = \dfrac{\beta - \xi(d/l)}{\left[\beta + (d/l)^2\right]^{3/2}}$, with $\beta = 1 - \dfrac{1-\beta_0}{\cos\Theta}$. The three contributions to the shear stress are the "fiber-field" interaction (τ_m), friction (τ_{fr}) and fiber-fiber dipolar interaction (τ_d).

In order to check the effect of the dipolar interactions, we show in Figure 3 the stress-strain curves for magnetic fiber suspensions without dipolar interactions (equation 12) and with dipolar interactions (equation 16). Almost in the whole range of strain angles, the magnetic interaction between fibers lowers slightly the shear stress. This is because the fibers tend to be aligned end-by-end and, therefore, the columns tend to extend. The inclined columns, confined between two plates, push therefore the upper plate and facilitate the shear deformation of the suspension. At high strain angles, when the fiber extremities become closer, the magnetic attraction between the fiber poles increases. The normal component, f_{mn}, of the magnetic force becomes comparable with the tangential one, $f_{m\tau}$. The friction force increases too, being proportional to the normal force. Therefore, we observe a rapid growth of the shear stress close to end-by-end alignment (Figure 3). The yield stress corresponds to the global maximum of the stress-strain curve. It is reached either at the critical strain angle $\theta_c \approx 30^o$ for $\xi \le 0.7$, or at end-by-end alignment for higher friction coefficients, $\xi \ge 0.7$ (Figure 3).

III.2. ZIGZAG STRUCTURE

In reality, the fibers are not perfectly aligned but form a complicated network. One of the model structures with lower anisotropy is the one where the fibers are connected by their extremities, forming zigzag-like chains that span the gap between two parallel plates (Figure 4). Let the angle between the fibers and the magnetic field be δ_0 at zero strain (Figure 4a). When the suspension is sheared at a strain angle, Θ, the zigzag structures are supposed to be inclined in such a way that the axis of symmetry of each zigzag chain (the line joining fiber

centers) makes the angle Θ with the magnetic field (Figure 4b). We also suppose that all the fibers in the chain make the same angle, δ, with the axis of symmetry. This angle is found from geometrical considerations: $\cos\delta = \dfrac{\cos\delta_0}{\cos\Theta}$.

Each fiber is subjected to the magnetic torque and to the action of the contact and magnetic dipolar forces. If we assume the fibers to be sphero-cylinders, the fiber contact points will be located on the lines joining the centers of the end hemispheres of the neighboring fibers. Each of these lines is parallel to the chain axis of symmetry and, therefore, the normal contact force, f_n, and the magnetic force, f_m, are also parallel to this axis. In each zigzag chain, one half of the fibers make the angle $\Theta + \delta$ with the magnetic field, and the other half the angle $\Theta - \delta$. Neglecting the terms of the order of d/l, the balance of torques for these two kinds of fibers reads:

$$T_1 = (f_n - f_m)\, l \sin\delta + f_\tau l \cos\delta \tag{17}$$

$$T_2 = -(f_n - f_m)\, l \sin\delta + f_\tau l \cos\delta \tag{18}$$

Since both fibers make different angles with the magnetic field, they are subjected to different magnetic torques, T_1 and T_2. We have assigned the counter-clockwise direction to positive magnetic torques. Thus, in Figure 5, the torque T_1 is positive and T_2 is negative. It is important to note that, in the absence of friction between fibers, the torque balance (17), (18) can only be satisfied at zero strain, when $T_1 = -T_2$. The friction between fibers prevents their extremities from sliding over each other, so that the zigzag structure is not destroyed by the shear deformation. Furthermore, when the fiber extremities do not slide, the friction force, f_τ, is independent of the normal force f_n. It can take any value not exceeding the maximum, ξf_n. When the friction force becomes $f_\tau = \xi f_n$, the fiber extremities slide over each other until they detach and the structure breaks –this could correspond to the flow onset.

The magnetic torques T_1 and T_2 are defined by equation (11), in the same way as for the fibers in the column structure. We only have to replace in equation (11) the angle Θ by appropriate angles $\Theta + \delta$ and $\Theta - \delta$ and the magnetic susceptibility χ_f by the susceptibilities χ_{f1} and χ_{f2} of the first and the second type of fibers. Both χ_{f1} and χ_{f2} are functions of the magnetic field and are defined in the Appendix. The shear stress is given by the general expression (7) and, for the zigzag structure (always neglecting the terms of the order of d/l), this expression takes the form:

$$\tau = \frac{\Phi}{V_f}\left[-(f_n - f_m)\cos\Theta + f_\tau \sin\Theta\right]\cos\Theta\cos\delta \qquad (19)$$

Working out the forces, $(f_n - f_m)$ and f_τ, as functions of the torques, T_1 and T_2, using equations (17), (18), and replacing the torques by the appropriate relation (11), we arrive to the final expression for the shear stress:

$$\tau = \frac{1}{2}\Phi\mu_0 H^2 \sin(\Theta+\delta)\sin(\Theta-\delta)\frac{\cos\Theta}{\sin\delta}\left(\frac{{\chi_{f2}}^2}{2+\chi_{f2}}\cos(\Theta-\delta) - \frac{{\chi_{f1}}^2}{2+\chi_{f1}}\cos(\Theta+\delta)\right) \qquad (20)$$

Note that the friction coefficient does not intervene in the expression for the shear stress. This is because the fibers do not slide over each other. The friction force adapts its value to satisfy the mechanical equilibrium of the structure, which is totally defined by the magnetic torques acting on the fibers.

The stress-strain curves for fiber suspensions with zigzag structure are presented in Figure 6 for a magnetic field intensity, H_0 = 100 kA/m and for three different initial zigzag angles, δ_0 = 20º, 36º and 45º. We see that the shear stress is quite sensitive to the initial angle δ_0, but the shape of the stress-strain curves is the same for any δ_0. At low strain, the suspension develops a negative shear stress. This is because the fibers tend to align with the magnetic field, and they push each other in such a way that the zigzag chains tend to be straightened up. These chains act as compressed springs, and when they are inclined under

shear, they push the upper plate both upward and in the direction of the shear. This favors the shear deformation of the suspension. At the same time, the restoring magnetic torque acting on each chain hinders the structure deformation. At a strain angle large enough, the restoring effect of the magnetic torque becomes dominant and the shear stress positive, undergoing a rapid growth with the strain (Figure 6). Once it is positive, the shear stress for the zigzag structure grows monotonically with the strain angle until the zigzag chains extend completely and become straight chains (Figure 4d). At this point, corresponding to a strain angle $\Theta = \delta_0$, the zigzag structure becomes unstable and the fiber suspension begins to flow (Figure 4e). Alternatively, if the friction force between fiber extremities, f_τ, reaches its maximum, ξf_n, the structure loses its stability at lower strains (Figure 4c). In this case, as mentioned above, the fiber extremities slide over each other and the structure breaks at a critical angle, Θ_c, defined by the condition $f_\tau = \xi f_n$. Therefore, the yield angle is the minimum angle between Θ_c and δ_0: $\Theta_Y = \min[\Theta_c\ ,\ \delta_0]$. In order to determine the critical angle, Θ_c, the following formulas are used:

$$f_n = \frac{\mu_0 H^2 V_f}{4l\sin\delta}\left(\frac{\chi_{f1}^{\ 2}}{2+\chi_{f1}}\sin 2(\Theta+\delta) - \frac{\chi_{f2}^{\ 2}}{2+\chi_{f2}}\sin 2(\Theta-\delta)\right) + f_m, \qquad (21)$$

$$f_\tau = \frac{\mu_0 H^2 V_f}{4l\cos\delta}\left(\frac{\chi_{f1}^{\ 2}}{2+\chi_{f1}}\sin 2(\Theta+\delta) + \frac{\chi_{f2}^{\ 2}}{2+\chi_{f2}}\sin 2(\Theta-\delta)\right), \qquad (22)$$

$$f_m = \frac{m_1 m_2}{4\pi\mu_0 d^2 l^2} = \frac{\mu_0 \chi_{f1}\chi_{f2} H^2 V_f}{16l}\left\{\left[\cos^2(\Theta+\delta)+\sin^2(\Theta+\delta)\left(\frac{1+\chi_\perp/2}{1+\chi_{f1}/2}\right)^2\right]\left[\cos^2(\Theta-\delta)+\sin^2(\Theta-\delta)\left(\frac{1+\chi_\perp/2}{1+\chi_{f2}/2}\right)^2\right]\right\}^{1/2} \qquad (23)$$

The magnetic susceptibilities, χ_{f1}, χ_{f2}, and $\chi_{\perp}$, as well as the internal magnetic field, are calculated in the Appendix. The yield stress for the zigzag structure is calculated using equation (20) by replacing the strain angle, Θ, by the yield angle Θ_Y.

III.3. 3D FIBER NETWORK

Both models studied above (column and the zigzag structures) are, of course, ideal representations of the real fiber structure. In the present section, we will consider a 3D network of the fiber suspension with a stochastic distribution of fiber orientations (Figure 7a), like the one observed in experiments (cf. Figure 8 of the companion paper). As in the previous models, the fiber suspension is sandwiched between two horizontal infinite planes and subjected to a magnetic field normal to the planes. Let us consider a shear deformation of the suspension by a strain angle Θ, in the yz-plane. The fiber network deforms under strain, and the fibers displace and pivot relatively to each other, their orientations being described by the polar angle θ and the azimuthal angle φ. We make the following assumptions:

1. The fibers are long cylinders: $l/d >> 1$.

2. The effect of the magnetic field created by neighboring fibers on the magnetization of a given fiber is taken into account by considering that each fiber is placed in an effective medium with the mean magnetic field, *H*, calculated by the mean field theory (see the Appendix).

3. As in the case of the column and zigzag structures, both mechanical contact and dipolar magnetic interactions are considered to be point-wise.

In equilibrium, all forces applied to each fiber must satisfy the force and the torque balance:

$$\sum_i \mathbf{f}_i = 0\,, \tag{24}$$

$$\mathbf{T}_m + \sum_i \mathbf{r}_i \times \mathbf{f}_i = \mathbf{0}. \tag{25}$$

Here $\mathbf{r}_i$ is the vector connecting the fiber center with the point of application of the force $\mathbf{f}_i$. If the fibers are considered to be infinitely thin, the vector $\mathbf{r}_i$ is parallel to the fiber. We can decompose the forces acting on the fibers into the components $f_{x'}$, $f_{y'}$, $f_{z'} = f_{||}$, along the axes of the coordinate frame Ox'y'z' attached to a given fiber (Figure 7b). The magnetic torque vector, $\mathbf{T}_m = \mathbf{m} \times \mathbf{H}$, is perpendicular to the plane Ozz' formed by the fiber and the magnetic field vector **H**, and is parallel to the Oy' axis of the fiber reference frame (Figure 7b). Projections of the torques onto the axes Ox' and Oy' give:

$$-\sum_i s_i f_{y'i} = 0\,, \tag{26}$$

$$-T_m + \sum_i s_i f_{x'i} = 0\,, \tag{27}$$

where the scalar T_m is defined by equation (11), s_i is the distance between the fiber center and the point of application of the force $\mathbf{f}_i$; $s_i > 0$ if the point of application of the corresponding force is located above the fiber center, and otherwise $s_i < 0$.

The shear stress of the fiber suspension is defined by the general expression (7), where the y-component of the force intervenes. Since the force $\mathbf{f}_i$ is decomposed into the components $f_{x'}$, $f_{y'}$ and $f_{||}$ along the axes of the fiber reference frame, the y-component of this force is the sum of the y-components of each individual term:

$$f_{yi} = \left(f_{x'}\right)_{yi} + \left(f_{y'}\right)_{yi} + \left(f_{||}\right)_{yi}. \tag{28}$$

From geometrical considerations (Figures 7b, c) we obtain: $\left(f_{x'}\right)_{yi} = f_{x'i}\cos\theta\sin\varphi$; $\left(f_{y'}\right)_{yi} = f_{y'i}\cos\varphi$, $\left(f_{||}\right)_{yi} = f_{||i}\sin\theta\sin\varphi$ and $r_{zi} = s_i\cos\theta$. Thus, using these expressions and replacing the force f_y by equation (28), the expression (7) for the shear stress takes the form:

$$\tau = \frac{1}{V}\sum_{\text{fibers}}\sum_i r_{zi} f_{yi} = \frac{1}{V}\sum_{\text{fibers}}\sum_i \left(s_i f_{x'i}\cos^2\theta\sin\varphi + s_i f_{y'i}\cos\theta\cos\varphi + s_i f_{||i}\cos\theta\sin\theta\sin\varphi\right) \tag{29}$$

Finally, taking into account the torque balance (equations 26, 27) and formula (11) for the torque T_m, the expression for the shear stress is written as:

$$\tau = \frac{1}{V}\sum_{\text{fibers}}\left(\frac{1}{2}\mu_0 \frac{\chi_f{}^2}{2+\chi_f} V_f H^2 \sin 2\theta \cos^2\theta \sin\varphi\right) + \frac{1}{2V}\sum_{\text{fibers}}\left(\sin 2\theta \sin\varphi \sum_i s_i f_{||i}\right) = \frac{1}{2}\Phi\mu_0 H^2 \left\langle \frac{\chi_f{}^2}{2+\chi_f} \sin 2\theta \cos^2\theta \sin\varphi \right\rangle + \frac{1}{2V}\sum_{\text{fibers}}\left(\sin 2\theta \sin\varphi \sum_i s_i f_{||i}\right) \quad (30)$$

The symbol $\langle ... \rangle$ denotes the averaging over a stochastic fiber orientation: $\langle ... \rangle = \int_0^{2\pi} d\varphi \int_0^{\pi} F(\varphi,\theta) \sin\theta \,(...)\, d\theta$, with $F(\varphi,\theta)$ being the orientation distribution function of fibers.

Formula (30) is pertinent to the calculation of the shear stress via direct particle-level simulations, planned for future work. For analytical calculations, it is required the knowledge of the distribution of the longitudinal forces exerted on the fibers, $f_{||i}$, as well as the angular distribution function of fiber orientations, $F(\varphi,\theta)$. At this moment, we do not know how to predict them rigorously with statistical or energy analyses. Nevertheless, we can perform analytical predictions of our theory for the near-planar stochastic structure by introducing some simplifications in the model.

III.4. NEAR-PLANAR STOCHASTIC STRUCTURE

Let us now suppose that all the fibers lie more or less in planes parallel to the shear plane. Thus, the fiber suspension can be represented as a series of sheets, each one parallel to the shear plane, and containing stochastically oriented fibers, as depicted in Figure 8a. We shall calculate the yield stress of such fiber network under the following considerations:

1. Analogously to the column structure, the magnetic dipolar forces are negligible and the only forces exerted on the fibers are the contact forces.

2. Most of the contact points are located on the lateral fiber surface rather than at the fiber extremities.

3. When the suspension is sheared, all the fibers slide over each other, with the Coulomb's friction force, $f_\tau = \xi f_n$. The two last assumptions were introduced by Toll and Manson (1994) for suspensions of very long nonmagnetic fibers.

4. Fibers contained in the same sheet touch each other in a few points and their contact forces are supposed to be parallel to the shear yz-plane. According to the second assumption, the friction force between fibers contained in the same sheet is parallel to the fiber major axis Oz'. Therefore, the longitudinal contact force between fibers of the same sheet is $f_{||i}^* = f_{\tau i}^* = \xi f_{ni}^*$.

5. Fibers contained in neighboring sheets have also a few mechanical contacts between them. Their normal contact forces, f_n^0, are supposed to be perpendicular to the shear yz-plane. Since the magnetic torque exerted on the fibers is in the shear plane, there is no magnetic torque in the xz-plane, and the normal contact forces, f_n^0, are compensated only by the magnetic dipolar forces between contacting fibers (Figure 8b). Tangential friction forces between fibers contained in different sheets lie in the shear yz-plane, and are equal to $f_{\tau i}^0 = \xi f_{ni}^0 \sim \xi f_m$. According to the first assumption, these friction forces are negligible compared to the friction forces between fibers of the same sheet: $f_{\tau i}^0 << f_{\tau i}^*$. Consequently, the longitudinal contact force acting on fibers will only include the friction forces between fibers contained in the same sheet: $f_{||i} = f_{||i}^* = \xi f_{ni}^*$.

By analogy with formula (27), the balance of torques acting on a given fiber in the shear yz-plane, reads:

$$-T_m + \sum_i s_i f_{ni}^* = 0\,, \tag{31}$$

Taking into account this expression, replacing the magnetic torque by formula (11) and setting $\varphi = \pi/2$, we arrive to the following expression for the shear stress of our near-planar structure:

$$\tau = \frac{1}{2}\Phi\mu_0 H^2 \left\langle \frac{\chi_f^{\,2}}{2+\chi_f} \sin 2\theta \cos^2\theta \right\rangle + \frac{1}{2V}\sum\nolimits_{\text{fibers}} \left(\xi T_m \sin 2\theta\right) = \frac{1}{2}\Phi\mu_0 H^2 \left\langle \frac{\chi_f^{\,2}}{2+\chi_f} \sin 2\theta \left(\cos^2\theta + \frac{1}{2}\xi \sin 2\theta \right) \right\rangle \tag{32}$$

6. The angular mean in Equation (32) is calculated via the angular distribution function of the near-planar structure: $\langle ... \rangle = \int_{-\pi/2}^{\pi/2} F(\theta)\,(...)\,d\theta$. The fiber orientation is supposed to be strongly influenced by the shear deformation, and the angular distribution function is assumed to be Gaussian and centered at the strain angle, Θ:

$$F(\theta) = \alpha_1 \exp[-\alpha_2 (\theta - \Theta)^2] \tag{33}$$

Hear α_1 and α_2 are the parameters of the distribution function. Furthermore, in the absence of shear the fiber distribution is considered to be isotropic in the yz-plane. When the strain is progressively increased, the fibers incline with the strain and get more aligned. At a threshold strain angle, Θ_a, the structure is supposed to be completely stretched, the straight fiber chains making the angle Θ_a with the magnetic field (Figure 1e). Under these conditions, the coefficient α_2 of the distribution function (equation 33) must be zero at zero shear, and infinite at the strain angle Θ_a. Then, this coefficient is supposed to be the following function of the strain: $\alpha_2 = \dfrac{\Theta}{\Theta_a - \Theta}$. The first coefficient, α_1, is found from the normalization condition: $\int_{-\pi/2}^{\pi/2} F(\theta)\,d\theta = 1$, i.e. $\alpha_1 = \left(\int_{-\pi/2}^{\pi/2} \exp\left[-\alpha_2 (\theta - \Theta)^2\right] d\theta \right)^{-1}$. Finally, the threshold

strain angle is set at $\Theta_a = 60^o$, which corresponds to the complete alignment of the column structure with the interfiber overlap $b_0 = 0.5l$ (or overlap parameter $\beta_0 = 0.5$).

The stress-strain curve obtained by this model is plotted in Figure 9 and compared with the corresponding curves obtained for the column and zigzag structures. In the same way as for the column structure, the stress-strain relation for the near-planar structure presents a local maximum, which corresponds to the yield stress. This maximum is observed at a strain angle close to the angle Θ_a of complete alignment of the structure. Note that the stress-strain curve departs from non-zero shear stress at zero strain. This is not surprising because we have assumed that, at any strain, all fibers slide over each other and experience the friction force, $f_\tau = \xi f_n$. At zero strain, the normal forces between randomly oriented fibers are not zero, leading to non-zero friction forces and thus to a non-zero contribution to the shear stress. In reality, when the fibers do not slide, the friction forces between them can take any value within the range: $-\xi f_n \le f_\tau \le \xi f_n$ –this is the case of the zigzag structure, where the friction forces between fiber extremities adapt their value to maintain the structure mechanically stable. Consequently, at small strain angles our model cannot predict with confident the shear stress of the near-planar structure. It is the reason why we have plotted the initial part of the stress-strain curve as a dashed line (Figure 9). On the other hand, at higher strain angles, when the random structure has been sufficiently strained, most of the fibers are expected to slide over each other, and the assumption $f_\tau = \xi f_n$ seems to be reasonable, at least for the estimation of the yield stress.

IV. DISCUSSION. COMPARISON WITH EXPERIMENTS

In the present section we compare the theoretical predictions of the models constructed above with the experimental values of the yield stress of fiber suspensions reported in the companion paper. Figure 10 shows the theoretical and experimental values of

the yield stress of fiber suspensions, plotted as a function of the external magnetic field, for four solid volume fractions, Φ = 0.01, 0.03, 0.05 and 0.07. The five curves in each graph correspond to the theoretical results using the models described in the present paper and the solid circles correspond to the experimental results reported in the companion paper. As observed in Figure 10, the highest estimation of the yield stress is given by the model of the column structure with friction (upper solid curve, cf. equation 12), and the lowest estimation by the model of the zigzag structure (lower solid curve, cf. equation 20). At magnetic fields $H_0 \geq 100$ kA/m, the experimental points lie between these two curves. At lower magnetic fields the experimental yield stress is higher than the one given by the highest theoretical estimation. This is possibly due to the underestimated value of the initial magnetic susceptibility used in our calculations, χ_i = 17.3. As mentioned in the companion paper, this value has been obtained by a fit of the experimental magnetization curve in the range of magnetic fields 45 – 4000 kA/m.

Comparing different theoretical predictions, we note that the yield stress for the column structure with the friction coefficient ξ = 1, is roughly two times higher than the yield stress for the same structure without friction. In the latter case, the yield stress is given by formula (17), which is very similar to the formula for the column structure of classical MR suspensions composed of spherical particles [Bossis et al. (1997)]. The authors of this paper calculated the stress as the derivative of the magnetic energy with respect to the shear strain: $\tau = \frac{\partial U_m}{\partial \gamma}$. The correspondence between our model and the one based on magnetic energy was expected in the limit case of zero friction, and is a test of the validity of our model.

As observed in Figure 10, the dipolar magnetic interactions between fibers do not give any significant contribution to the yield stress (dotted curve, cf. equation 16). In reality, the magnetic interactions between contacting fibers could be much stronger than those predicted

by the dipolar approximation. The multipolar approach [Klingenberg et al. (1991); Clercx and Bossis (1993)], direct numerical simulations [Bossis et al. (2003); López-López et al. (2006)] and other sophisticated models [Ginder et al. (1996); Bossis et al. (2002)] allowed to determine with precision the magnetic forces between spherical particles. Nevertheless, the dipolar approximation remains valid at high magnetic fields, when the magnetization of the particles is of the same order that the saturation magnetization. In our experiments we cover such range of magnetic fields ($H_0 \geq 200$ kA/m, cf. Figure 1 of the companion paper). Therefore, our conclusions made in the frame of the dipolar approximation remain valid, at least for this range of magnetic fields. At lower fields the magnetic attraction between fibers is underestimated and that could be another reason for the discrepancy between theoretical and experimental results at $H_0 \leq 100$ kA/m.

By analyzing the zigzag model we can identify the two reasons why this model predicts the lowest yield stress. Firstly, the strained zigzag chains act as compressed springs that push upward the rheometer plate (cf. Figure 4b). Secondly, this structure has a relatively low anisotropy compared to the column structure. The most realistic model –the model of the near-planar stochastic structure (equation 32)– gives a reasonable correspondence with the experiments at fiber volume fractions $\Phi = 0.05$ and 0.07 (Figures 10c-d). This model takes into account the friction between fibers as well as the progressive alignment of the fiber network with increasing strain.

Let us now analyze the effect of solid concentration on the yield stress of fiber suspensions. As observed in Figure 10, at fiber volume fractions $\Phi = 0.01$ and 0.03, the experimental points are closer to the prediction of the zigzag model. For more concentrated suspensions ($\Phi = 0.05$ and 0.07), the experiment is better described by the column structure model. One of the possible reasons for this behavior is a higher anisotropy of the more concentrated fiber suspensions. In fact, in more concentrated suspensions the fibers have less

free space to pivot. Consequently, as the solid concentration increases, the fiber network is supposed to approach a column structure. Nevertheless, whatever the fiber concentration, the column structure with perfect alignment of fibers can be realized only in the absence of friction. Note that the three inspected models –column structure, zigzag structure and near-planar structure– give almost linear concentration dependence of the yield stress. A small deviation from linearity is observed at low-to-moderate magnetic field (up to 100 kA/m). This is connected to the weak concentration dependence of the magnetic permeability of fiber suspensions, which intervenes in the expression for the internal magnetic field, *H* (cf. equation A.1). However, such magnetostatic effect cannot explain a power-law concentration dependence of the yield stress as high as that observed experimentally: $\tau_Y \propto \Phi^{1.5}$ (cf. companion paper). The linear concentration dependence in the column and the near-planar structure models comes mostly from the assumption that the friction force between fibers is longitudinal and always equal to ξf_n. In this case, in equation (30) the sum $\sum_i s_i f_{||i}$ over all the contact points on a given fiber is simply proportional to the magnetic torque acting on a considered fiber: $\sum_i s_i f_{||i} = \xi T_m$, whatever the number of contact points. Consequently, the theoretical yield stress is linear in the number of fibers per unit volume (i.e. in the concentration) rather than in the total number of contact points. However, in a real situation of the 3D stochastic structure described in Section III.3, the second term of the stress equation (30), $\frac{1}{2V}\sum_{\text{fibers}}\left(\sin 2\theta \sin\varphi \sum_i s_i f_{||i}\right)$, is not necessarily proportional to the magnetic torque and can hide a stronger concentration dependence. This is the case of isotropic suspensions of non-magnetic elastic fibers, for which the yield stress is proportional to the number of contact points per unit volume, which varies as the square of the solid volume fraction [Toll and Manson (1994); Servais et al. (1999)].

Note finally that the fiber friction coefficient, ξ, is the only unknown parameter in the models of the column and the near-planar stochastic structures. We plan to measure this coefficient in order to obtain a model free of unknown parameters.

V. CONCLUDING REMARKS

In this work, predictions of the yield stress of magnetic fiber suspensions in the presence of magnetic field have been performed for the first time, on the basis of new microstructural models. Our theory describes reasonably well the enhanced magnetorheological effect observed experimentally in magnetic fiber suspensions (companion paper), in terms of the interfiber solid friction. Different structures of fiber suspensions have been considered in this paper. The quasi-static regime of the shear deformation of each structure (before the flow onset) has been studied, and the suspension yield stress has been attributed to the structure failure at a critical strain.

The simplest column structure is expected at low interfiber friction and/or at high fiber volume fraction. Because of its high anisotropy, such structure gives the highest estimation of the yield stress of magnetic fiber suspensions. A more isotropic structure is obtained when the fibers form zigzag chains, which can act as compressed springs, restoring their energy and decreasing the stress. Such zigzag structure gives the lowest estimation of the yield stress. In the more realistic near-planar stochastic structure the fibers are supposed to lie more or less in planes parallel to the shear plane and to be stochastically oriented within these planes. We have introduced a Gaussian distribution function of fiber orientations centered at the strain angle. The yield stress predicted by this model is closer to the one predicted by the column structure model than to that predicted by the zigzag structure model.

We have also developed an effective medium theory for the real 3D stochastic fiber network. This theory does not give an analytical prediction for the yield stress, but gives a

general expression for the shear stress as a function of the mean magnetic torque exerted on the fibers and the contact forces parallel to the fiber axis. Particle level simulations will be performed in the future to investigate the behavior of such 3D network under shear.

In all the models, we have found that the two main contributions to the yield stress of magnetic fiber suspensions come from the magnetic torque and from the friction force, while the dipolar magnetic interaction between fibers plays a minor role. Nevertheless, a numerical simulation (by finite element methods) of the magnetic interactions will be conducted in the future to verify the validity of the dipolar approach used in the present work.

Finally, the three considered models predict almost linear concentration dependence of the yield stress of fiber suspensions in the presence of magnetic field, while a dependence on $\Phi^{1.55}$ was observed in experiments (companion paper). This discrepancy comes from the assumption that the friction force between fibers is equal to ξf_n, which will be corrected in our future work. Despite this discrepancy, our theory covers a quite wide range of the rheological phenomena observed in the new and promising magnetorheological fiber suspensions.

ACKNOWLEDGMENTS

The authors would like to kindly thank Prof. Andrey Zubarev and Dr. Sandris Lacis for helpful discussions. Eureka E! 3733 Hydrosmart project and “Conseil Régional PACA” (Biomag project) are acknowledged for their financial support. One of the authors (M.T.L.-L.) also acknowledges financial support by Secretaría de Estado de Universidades e Investigación (Postdoctoral Fellowship Program, MEC, Spain) and by the University of Granada (Spain).

APPENDIX: CALCULATION OF THE MAGNETIC FIELD INSIDE THE FIBER SUSPENSION

The magnetic field intensity inside a thin layer of fiber suspension sandwiched between two plates is given by: $H = \frac{H_0}{\mu_{zz}}$, whatever the structure of the suspension. Here H_0 is the external magnetic field intensity and μ_{zz} is the *zz*-component of the permeability tensor of the fiber suspension. The magnetic permeability of the suspension depends on the fiber magnetic properties, the fiber volume fraction of the suspension and the geometry of the suspension structure, i.e. the arrangement of fibers in the suspension. Let us consider first the column structure of fiber suspensions, for which μ_{zz} is related to the permeability components along the major and minor fiber axes, $\mu_{||}$ and $\mu_{\perp}$, through the expression: $\mu_{zz} = \mu_{||}\cos^2\Theta + \mu_{\perp}\sin^2\Theta$. Hence, the internal magnetic field is:

$$H = \frac{H_0}{\mu_{||}\cos^2\Theta + \mu_{\perp}\sin^2\Theta}. \qquad \text{(A.1)}$$

We determine $\mu_{||}$ and $\mu_{\perp}$ using Maxwell-Garnett mean field theory [Berthier (1993)] in the same way as it was done by Bossis et al. (1997) for the column structure composed of spherical particles:

$$\mu_{||} = 1 + \chi_{||} = 1 + \Phi\chi_f, \qquad \text{(A.2)}$$

$$\mu_{\perp} = 1 + \chi_{\perp} = \frac{1 + \Phi\frac{\chi_f}{2 + \chi_f}}{1 - \Phi\frac{\chi_f}{2 + \chi_f}}. \qquad \text{(A.3)}$$

In the general case, the fiber susceptibility, χ_f, is a function of the magnetic field inside the fiber, H_f. To get this function, we fitted the experimental magnetization curve (cf. Figure 1 of the companion paper) to the Fröhlich-Kennelly formula [Jiles (1991)]. The expressions for χ_f and H_f read:

$$\chi_f = \frac{\chi_i M_s}{M_s + \chi_i H_f}, \tag{A.4}$$

$$H_f = H\sqrt{\cos^2\Theta + \sin^2\Theta\left(\frac{1+\chi_\perp/2}{1+\chi_f/2}\right)^2}\ . \tag{A.5}$$

Here χ_i = 17.3 and M_s = 1366 kA/m are the initial magnetic susceptibility and the saturation magnetization of fibers, respectively. The simultaneous resolution of equations (A.1)–(A.5) gives us the values of χ_f, H_f and H at given external magnetic field H_0, strain angle Θ and concentration Φ.

Using Maxwell-Garnett theory, we also get the magnetic permeability of fiber suspensions with zigzag structure. The internal magnetic field is given by formula (A.1) with $\mu_{||}$ and $\mu_\perp$ being the components of the magnetic permeability tensor along the main axes of the zigzag chains, Oz' and Oy' (cf. Figure 5):

$$\mu_{||} = 1 + \chi_{||} = \frac{1+\Phi(1-N_{||})\beta_{||}}{1-\Phi N_{||}\beta_{||}}, \tag{A.6}$$

$$\mu_\perp = 1 + \chi_\perp = \frac{1+\Phi(1-N_\perp)\beta_\perp}{1-\Phi N_\perp\beta_\perp}, \tag{A.7}$$

with $N_{||} = \frac{1}{2}\sin^2\delta$, $N_\perp = \frac{1}{2}\cos^2\delta$ and $\beta_{||}$, $\beta_\perp$ being given by the following expressions:

$$\beta_{||} = \frac{1}{2}\left(\frac{\chi_{f1}}{1+N_{||}\chi_{f1}} + \frac{\chi_{f2}}{1+N_{||}\chi_{f2}}\right) = \frac{\chi_{f1}}{2+\chi_{f1}\sin^2\delta} + \frac{\chi_{f2}}{2+\chi_{f2}\sin^2\delta}, \tag{A.8}$$

$$\beta_\perp = \frac{1}{2}\left(\frac{\chi_{f1}}{1+N_\perp\chi_{f1}} + \frac{\chi_{f2}}{1+N_\perp\chi_{f2}}\right) = \frac{\chi_{f1}}{2+\chi_{f1}\cos^2\delta} + \frac{\chi_{f2}}{2+\chi_{f2}\cos^2\delta}. \tag{A.9}$$

Here the subscripts "1" and "2" correspond respectively to the fibers making the angle $\Theta+\delta$ and $\Theta-\delta$ with the magnetic field. The fiber susceptibilities, χ_{f1} and χ_{f2}, are functions of the magnetic fields inside the fibers, H_{f1} and H_{f2}, and are defined by equations (A.4)–(A.5),

where the angle Θ must be replaced by $\Theta+\delta$ for H_{f1} and $\Theta-\delta$ for H_{f2}. Resolving the system of equations (A.1, A.4, A.5, A.6, A.7) we get the magnetic parameters χ_{f1}, χ_{f2}, H_{f1}, H_{f2} and H as functions of the applied magnetic field, H_0, and the angles Θ and δ.

Finally, the magnetic field inside isotropic fiber suspensions is given by: $H=\dfrac{H_0}{\langle\mu\rangle}$, with the mean magnetic permeability, $\langle\mu\rangle$, defined by formula (A.10) for the 3D isotropic structure [Kuzhir et al. (2003)] and (A.11) for the planar (2D) isotropic structure:

$$\langle\mu_{3D}\rangle=\frac{1+\Phi\left[\frac{1}{3}(1-N_{||})\beta_{||}+\frac{2}{3}(1-N_{\perp})\beta_{\perp}\right]}{1-\Phi\left[\frac{1}{3}N_{||}\beta_{||}+\frac{2}{3}N_{\perp}\beta_{\perp}\right]}=\frac{3(2+\chi_f)+\Phi\chi_f(4+\chi_f)}{6+\chi_f(3-2\Phi)}, \qquad \text{(A.10)}$$

$$\langle\mu_{2D}\rangle=\frac{1+\Phi\left[\frac{1}{2}(1-N_{||})\beta_{||}+\frac{1}{2}(1-N_{\perp})\beta_{\perp}\right]}{1-\Phi\left[\frac{1}{2}N_{||}\beta_{||}+\frac{1}{2}N_{\perp}\beta_{\perp}\right]}=\frac{2(2+\chi_f)+\Phi\chi_f(3+\chi_f)}{4+\chi_f(2-\Phi)}. \qquad \text{(A.11)}$$

In these formulas, $N_{||}=0$ and $N_{\perp}=1/2$ are the demagnetization factors of the fiber; $\beta_{||}=\chi_f$ and $\beta_{\perp}=\dfrac{\chi_f}{1+\chi_f/2}$. The fiber magnetic susceptibility, χ_f, is obtained from equation (A.4), where we must replace H_f by the mean magnetic field inside the fibers, $\langle H_f\rangle$. For the 3D isotropic and planar structures this field is calculated by averaging the magnetic field H_f (equation A.5) over random fiber orientations. Note finally that, due to the saturation effects, the magnetic permeability of the fiber suspension decreases significantly when the external magnetic field is increased. At field $H_0 \geq 200$ kA/m, and for a fiber volume fraction $\Phi \leq 0.07$, the magnetic permeability of the suspension is not far from unity and, consequently, the internal magnetic field, H, is quite close to the external one, H_0.

REFERENCES

Aoshima, M. and A. Satoh, "Two-dimensional Monte Carlo simulations of a colloidal dispersion composed of rod-like ferromagnetic particles in an applied magnetic field," Model. Simul. Mater. Sci. Eng. **16**, 015004 (2008).

Batchelor, G. K., "The stress system in a suspension of force-free particles," J. Fluid Mech. **41**, 545-570 (1970).

Batchelor, G. K., "The stress generated in a non-dilute suspension of elongated particles by pure straining motion," J. Fluid Mech. **46**, 813-829 (1971).

Bell, R. C., J. O. Karli, A. N. Vavreck, D. T. Zimmerman, G.T. Ngatu and N.M. Wereley, "Magnetorheology of submicron diameter iron microwires dispersed silicon oil," Smart. Mater. Struct. 17, 015028 (2008).

Bennington, C. P. J., R. J. Kerekes and J. R. Grace, "The yield stress of fiber suspensions," Can. J. Chem. Eng. 68, 748-757 (1990).

Berthier, S., Optique des milieux composites. Polytechnica, Paris, 1993.

Bossis, G., E. Lemaire, O. Volkova and H. Clercx, "Yield stress in magnetorheological and electrorheological fluids: A comparison between microscopic and macroscopic structural models," J. Rheol. **41**, 687-704 (1997).

Bossis, G., O. Volkova, S. Lacis and A. Meunier, in “Ferrofluids,” Magnetorheology: Fluids, Structures and Rheology. S. Odenbach, ed., Springer, Berlin, 2002.

Bossis, G., P. Khuzir, S. Lacis and O. Volkova, “Yield behavior of magnetorheological suspensions,” J. Magn. Magn. Mater. **258**, 456-458 (2003).

Brenner, H., “Rheology of a dilute suspension of axisymmetric Brownian particles,” Int. J. Multiphase Flow **1**, 195-341 (1974).

Clercx, H. J. H. and G. Bossis, “Many-body electrostatic interactions in electrorheological fluids,” Phys. Rev. E **48**, 2721-2738 (1993).

Djalili-Moghaddam, M. and S. Toll, “A model for short-range interactions in fibre suspensions,” J. Non-Newton. Fluid Mech. **132**, 73-83 (2005).

Doi, M. and S. F. Edwards, The theory of Polymer Dynamics. Oxford Press, New York, 1986.

Folgar, F. and C. L. Tucker, “Orientation Behavior of Fibers in Concentrated Suspensions,” J. Reinforced Plast. Composites **3**, 98-119 (1984).

Ganani E., and R. L. Powell, “Suspensions of rodlike particles – literature-review and data correlations,” J. Compos Mater. **19**, 194-215 (1985).

Ginder, J. M., “Behavior of magnetorheological fluids,” MRS Bull **(Aug)** 26–29 (1998).

Ginder, J. M., L. C. Davis and L. D. Elie, “Rheology of magnetorheological fluids: Models and measurements,” Int. J. Mod. Phys. B **10**, 3293-3303 (1996).

Hinch, E. J. and L. G. Leal, “Time-dependent shear flows of a suspension of particles with weak Brownian rotations,” J. Fluid Mech. **57**, 753-767 (1973).

Hovarth, A. E. and T. Lindstrom, “The influence of colloidal interactions on fiber network strength,” J. Colloid Interface Sci. **309**, 511-517 (2007).

Jeffery, G. B., “The motion of ellipsoidal particles immersed in a viscous fluid,” Proc. R. Soc. Lond. A **102**, 161-179 (1922).

Jiles, D., Introduction to Magnetism and Magnetic Materials. Chapman & Hill, London, 1991.

Joung, C. G., N. Phan-Thien and X. J. Fan, “Direct simulation of flexible fibers,” J. Non-Newton. Fluid Mech. **99**, 1-36 (2001).

Klingenberg, D. J., F. van Swol and C. F. Zukoski, “The small shear rate response of electrorheological suspensions. 2. Extension beyond the point-dipole limit,” J. Chem. Phys. **94**, 6170-6178 (1991).

Kuzhir, P., G. Bossis, V. Bashtovoi and O. Volkova, “Flow of magnetorheological fluid through porous media,” Eur. J. Mech. B-Fluids **22**, 331-343 (2003).

Kuzhir, P., M. T. López-López, G. Vertelov, C. Pradille and G. Bossis, “Shear and squeeze rheometry of suspensions of magnetic polymerized chains,” Rheol. Acta (2007) in press. DOI 10.1007/s00397-007-0230-7

Landau, L. D. and E. M. Lifshitz, Electrodynamics of Continuous Media. Pergamon, New York, 1960.

Larson, R. G., The Structure and Rheology of Complex Fluids. Oxford University Press, New York, 1999.

Lindstrom, S. B. and T. Uesaka, “Simulation of the motion of flexible fibers in viscous fluid flow,” Phys. Fluids **19**, 113307 (2007).

López-López, M. T., G. Vertelov, G. Bossis, P. Kuzhir and J. D. G. Durán, “New magnetorheological fluids based on magnetic fibers,” J. Mater. Chem. **17**, 3839-3844 (2007).

López-López, M. T., P. Kuzhir, S. Lacis, G. Bossis, F. González-Caballero and J.D.G. Durán, “Magnetorheology for suspensions of solid particles dispersed in ferrofluids,” J. Phys.: Condens. Matter **18**, S2803-S2813 (2006).

López-López M.T., Kuzhir P., Bossis G. and Mingalev P. Preparation of well dispersed magnetorheological fluids and effect of dispersion on their magnetorheological properties. Rheol. Acta, **47**, 787-796 (2008).

Maiorov, M. M., “Measurement of the ferrofluid viscosity in magnetic field,” Magnetohydrodynamics **16**, 339-344 (1980).

Ngatu G.T., N.M. Wereley, J. O. Karli and R. C. Bell, “Dimorphic magnetorheological fluids: exploiting partial substitution of microspheres by nanowires,” Smart. Mater. Struct. 17, 040522 (2008).

Petrich M. P. and D. L. Koch, “Interactions between contacting fibers,” Phys. Fluids **10**, 2111-2113 (1998).

Petrie, C. J. S., “The rheology of fibre suspensions,” J. Non-Newton. Fluid Mech. **87**, 369-402 (1999).

Philipse, A. P. and A. M. Wierenga, “On the Density and Structure Formation in Gels and Clusters of Colloidal Rods and Fibers,” Langmuir **14**, 49-54 (1998).

Powell, R. L., “Rheology of Suspensions of Rodlike Particles,” J. Stat. Phys. **62**, 1073-1094 (1990).

Qi, D., “Direct simulations of flexible cylindrical fiber suspensions in finite Reynolds number flows,” J. Chem. Phys. 125, 114901 (2006).

Rahnama, M., D. L. Koch and E. S. G. Shaqfeh, “The effect of hydrodynamic interactions on the orientation distribution in a fiber suspension subject to simple shear flow,” Phys. Fluids **7**, 487-506 (1995).

Rubí, J. M., C. Salueña and A. Pérez-Madrid, “The viscosity of a suspension of elongated magnetic dipoles,” J. Magn. Magn. Mater. **122**, 193-195 (1993).

Salueña, C., A. Pérez-Madrid and J. M. Rubí, “The viscosity of a suspension of ferromagnetic rod-like particles,” J. Colloid Interface Sci. **164**, 269-279 (1994).

Satoh, A., “Rheological properties and orientational distributions of dilute ferromagnetic spherocylinder particle dispersions - Approximate solutions by means of Galerkin’s method,” J. Colloid Interface Sci. **234**, 425-433 (2001).

Satoh, A., “Rheological properties and particle behaviors of a nondilute colloidal dispersion composed of ferromagnetic spherocylinder particles subjected to a simple shear flow (analysis by means of mean-field approximation),” J. Colloid Interface Sci. **262**, 263-273 (2003).

Satoh, A., “Influence of magnetic interactions between clusters on particle orientational characteristics and viscosity of a colloidal dispersion composed of ferromagnetic spherocylinder particles: Analysis by means of mean field approximation for a simple shear flow,” J. Colloid Interface Sci. **289**, 276-285 (2005).

Schmid, C. F. and D. J. Klingenberg, “Mechanical Flocculation in Flowing Fiber Suspensions,” Phys. Rev. Lett. **84**, 290-293 (2000).

Schmid, C. F., L. H. Switzer and D. J. Klingenberg, “Simulations of fiber flocculation: Effects of fiber properties and interaction friction,” J. Rheol. **44**, 781-809 (2000).

Shaqfeh, E. S. G. and G. H. Fredrickson, “The hydrodynamic stress in a suspension of rods,” Phys. Fluid A **2**, 7-24 (1990).

Servais C., J.-A. E. Manson and S. Toll, “Fiber-fiber interaction in concentrated suspensions: Disperse fibers,” J. Rheol. **43**, 991-1004 (1999).

Servais, C., A. Luciani and J.-A. E. Manson, “Squeeze flow of concentrated long fibre suspensions: experiments and model,” J. Non-Newton. Fluid Mech. **104**, 165-184 (2002).

Shulman, Z. P. and W. I. Kordonsky, Magnetorheological effect. Nauka i Tehnika, Minsk, 1982 (in Russian).

Shulman, Z. P., “Magnetorheological systems,” in Magnetic Fluids and Applications Handbook. B. Berkovski and V. Bashtovoi, eds., Begell House, New York, 1996.

Switzer, L. H. and D. J. Klingenberg, “Flocculation in simulations of sheared fiber suspensions,” Int. J. Multiphase Flow **30**, 67-87 (2004).

Toll, S. and J.-A. E. Manson, “Dynamics of a planar concentrated fiber suspension with non-hydrodynamic interaction,” J. Rheol. 38, 985-997 (1994).

Tsebers, A. O., “Simulation of the magnetic rheology of a dilute suspension of ellipsoidal particles in a numerical experiment,” Magnetohydrodynamics **20**, 349-353 (1984).

Volkova, O., “Study of rheology of suspensions of magnetic particles,” Ph.D. Thesis, Université de Nice-Sophia Antipolis, 1998.

Wierenga, A., A. P. Philipse, H. N. W. Lekkerkerker and D. V. Boger, “Aqueous Dispersions of Colloidal Boehmite: Structure, Dynamics, and Yield Stress of Rod Gels,” Langmuir **14**, 55-65 (1998).

Winslow, W. M., “Induced fibration of suspensions,” J. Appl. Phys. 20, 1137-1140 (1949).

Yamamoto, S. and T. Matsuoka, “Dynamic simulation of fiber suspensions in shear flow,” J. Chem. Phys. **102**, 2254-2260 (1995).

Zirnsak M. A., D. U. Hur and D. V. Boger, “Normal stresses in fiber suspensions,” J. Non-Newton. Fluid Mech. **54**, 153-193 (1994).

Zubarev, A. Yu. and L. Yu. Iskakova, “Yield stress in thin layers of ferrofluids,” Physica A **365**, 265-281 (2006).

FIGURE CAPTIONS

Figure 1. Column structure behavior. At zero strain (a), the columns are aligned with the magnetic field. When the suspension is sheared (b), the columns are inclined at an angle Θ. Further shearing brings the structure either to the maximum of the shear stress (c) and the structure breaks (d) or to the end-by-end alignment (e).

Figure 2. Geometry of the column structure model. a) fibers aligned with the field at zero strain; b) fibers inclined at a strain angle, Θ (no dipolar interactions between fibers); c) dipolar forces between fibers.

Figure 3. Shear stress, τ, versus shear strain angle, Θ, calculated using the column structure model. Solid lines: calculations without dipolar interactions; dash lines: with dipolar interactions. Lower lines: no friction (ξ = 0); upper lines: friction with ξ = 1. The vertical dotted line corresponds to the end-by-end alignment of the fibers. For all the curves, the magnetic field intensity is H_0 = 100 kA/m, the dimensionless overlap is β_0 = 0.5 and the fiber aspect ratio is $l/d = 10$.

Figure 4. Zigzag structure behavior. At zero strain (a), the fibers gather in zigzag chains spanning the gap. When the suspension is sheared (b), the chains are inclined at the angle Θ and extend along their axis of symmetry. At further shearing, the structure becomes unstable, either when the friction force reaches its maximum (c), or when the zigzag chains extend completely (d). The structure breaks causing the flow of the fiber suspension (e).

Figure 5. Geometry of the zigzag structure model. a) zigzag chain at zero strain; b), c) inclined chain at strain angle Θ. The forces and torques acting on the most inclined fibers and the less inclined fibers are illustrated in (b) and (c), respectively.

Figure 6. Theoretical results of the zigzag structure model: stress-strain curve for three initial zigzag angles, δ_0 = 20º, 36º and 45º, and for a magnetic field intensity H_0 = 100 kA/m. The zigzag structure with the angle δ_0 = 45º breaks before reaching complete alignment –the dotted part of the curve indicates the inaccessible stress/strain region. The dashed arrows indicate the points corresponding to the yield stress.

Figure 7. Geometry of the 3D fiber network. a) network sheared in the yz-plane by a strain angle Θ –the fiber orientation is defined by the angles θ (≠Θ) and φ; b) sketch of forces and torques acting on a fiber; c) sketch explaining the magnitudes *r* and *s*, which characterize the location of the points of force application (solid circles in the fiber). The gray plane denotes the plane Ox'z'z, where the magnetic torque is exerted.

Figure 8. Geometry of the near-planar structure. a) The fiber network can be "sliced" into sheets parallel to the shear yz-plane. b) Projection of the fiber network onto the xz-plane. The fibers of the back sheet exert normal contact forces, f_n^0, on the fibers of the front sheet.

Figure 9. Stress-strain curve for column, zigzag and near-planar stochastic structure of a fiber suspension at magnetic field intensity H_0 = 100 kA/m, fiber volume fraction Φ = 0.05, and friction coefficient ξ = 1. The dipolar magnetic forces are neglected in all three cases. The initial zigzag angle for the zigzag structure is δ_0 = 30º.

Figure 10. Yield stress of fiber suspensions versus external magnetic field intensity, H_0, for different fiber volume fractions, Φ: (a) $\Phi = 0.01$; (b) $\Phi = 0.03$; (c) $\Phi = 0.05$; and (d) $\Phi = 0.07$. The upper and the middle solid lines correspond to the model of the column structure with $\xi = 1$ (equation 12) and $\xi = 0$ (equation 14), respectively; dotted line: same model but with dipolar magnetic interactions (equation 16) and with $\xi = 1$, $\beta_0 = 0.5$ and $l/d = 10$; lower solid line: model of the zigzag structure (equation 20) with $\xi = 1$ and $\delta_0 = 30^o$; dashed line: model of the near-planar stochastic structure (equation 32) with $\xi = 1$; solid circles: experimental data.

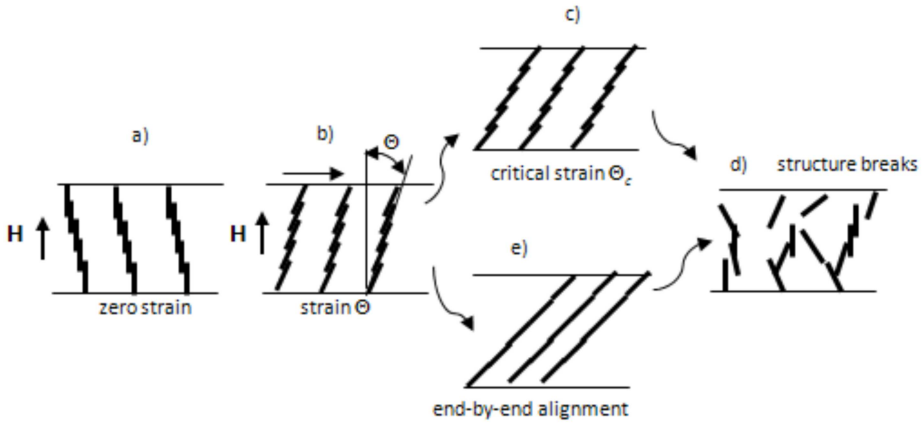
a)
b)
c)
d)
e)
H
H
Θ
zero strain
strain Θ
critical strain Θ_c
structure breaks
end-by-end alignment

Fig.1

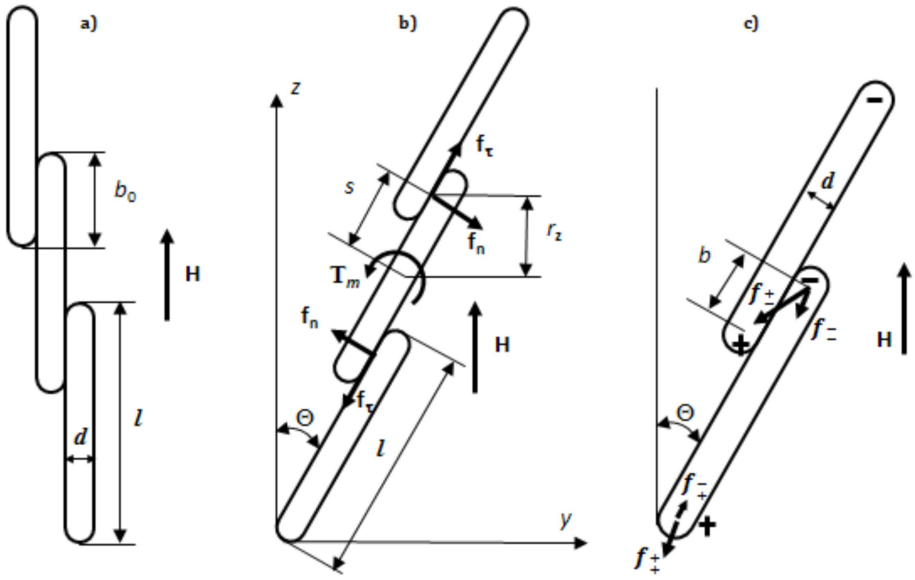

Fig.2

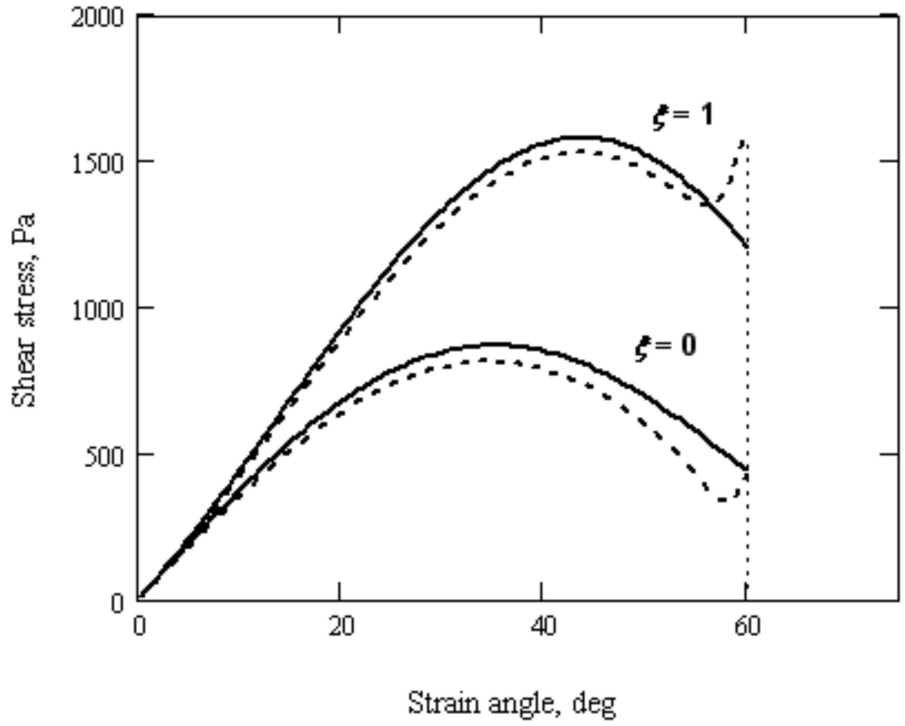
2000
1500
1000
500
0
Shear stress, Pa
ξ = 1
ξ = 0
0
20
40
60
Strain angle, deg

Fig.3

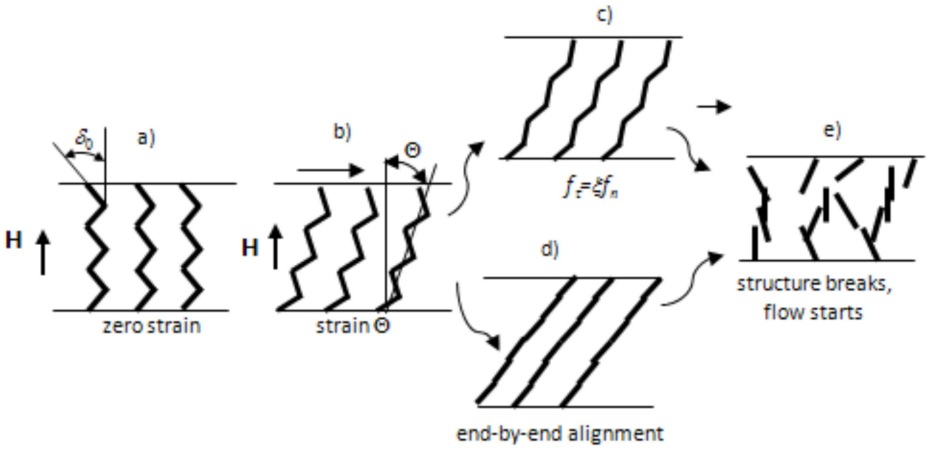
a)
b)
c)
d)
e)
H
H
zero strain
strain Θ
$f_t = \xi f_n$
end-by-end alignment
structure breaks,
flow starts

Fig.4.

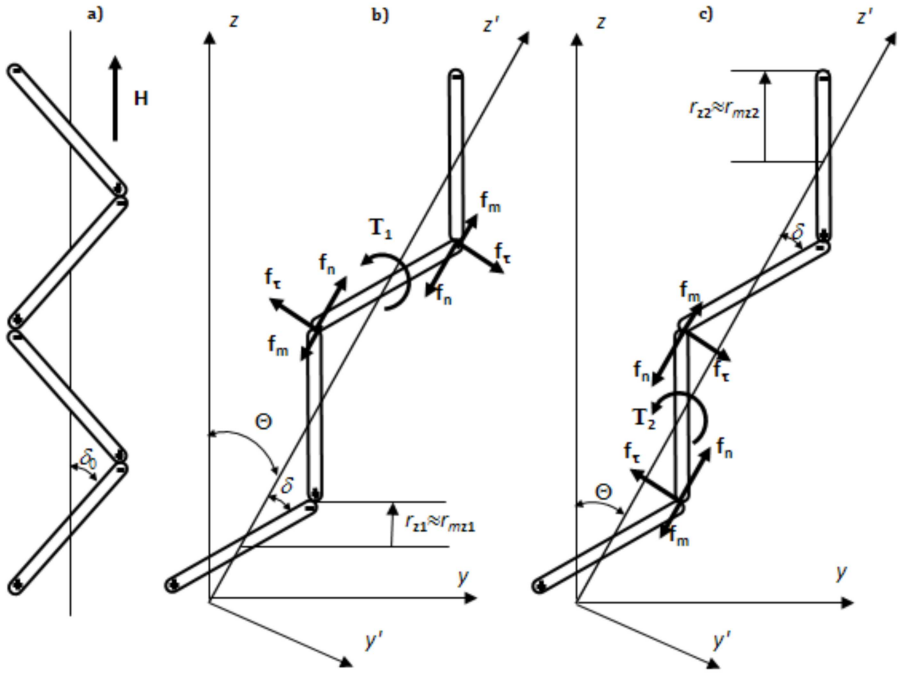
a)
H
δ_0
z
b)
z'
T_1
f_m
f_τ
f_n
f_τ
f_n
f_m
Θ
δ
$r_{z1} \approx r_{mz1}$
y
y'
z
c)
z'
$r_{z2} \approx r_{mz2}$
δ
f_m
f_n
f_τ
T_2
f_τ
f_n
Θ
f_m
y
y'

Fig.5

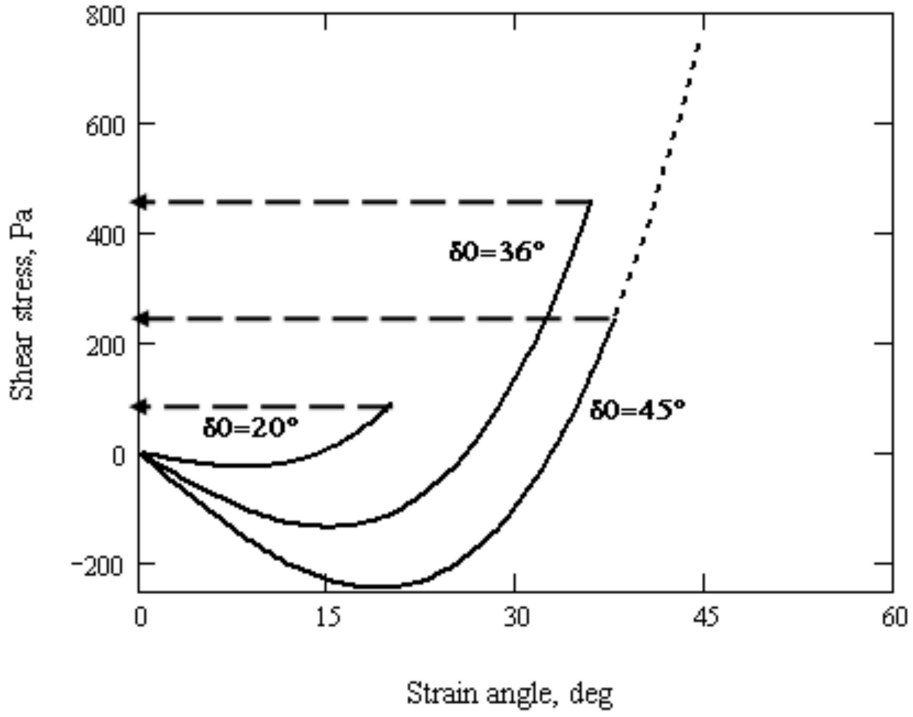
800
600
400
200
0
-200
Shear stress, Pa
δ0=36°
δ0=20°
δ0=45°
0
15
30
45
60
Strain angle, deg

Fig.6

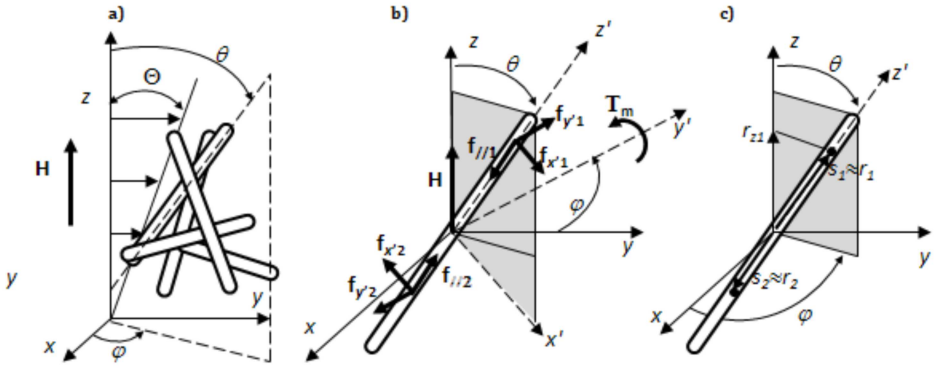
a)
b)
c)
θ
Θ
z
H
y
x
φ
z'
y'
x'
$f_{y'1}$
$f_{x'1}$
$f_{//1}$
T_m
$f_{x'2}$
$f_{y'2}$
$f_{i/2}$
r_{z1}
$s_1 \approx r_1$
$s_2 \approx r_2$

Fig.7

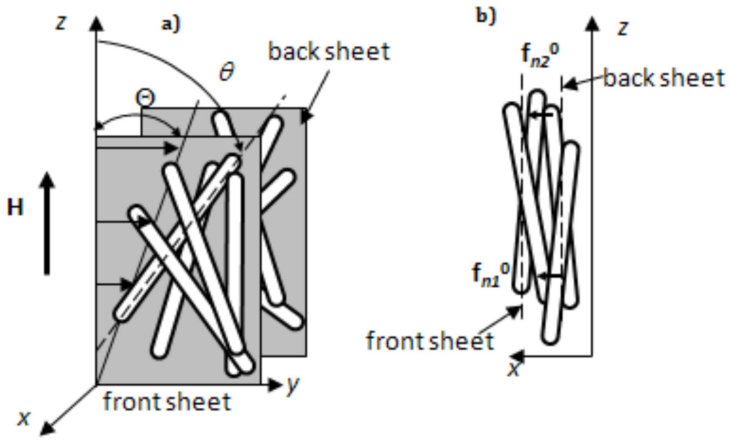
z
a)
back sheet
θ
Θ
H
front sheet
x
y
b)
z
f_{n2}^0
back sheet
f_{n1}^0
front sheet
x

Fig.8

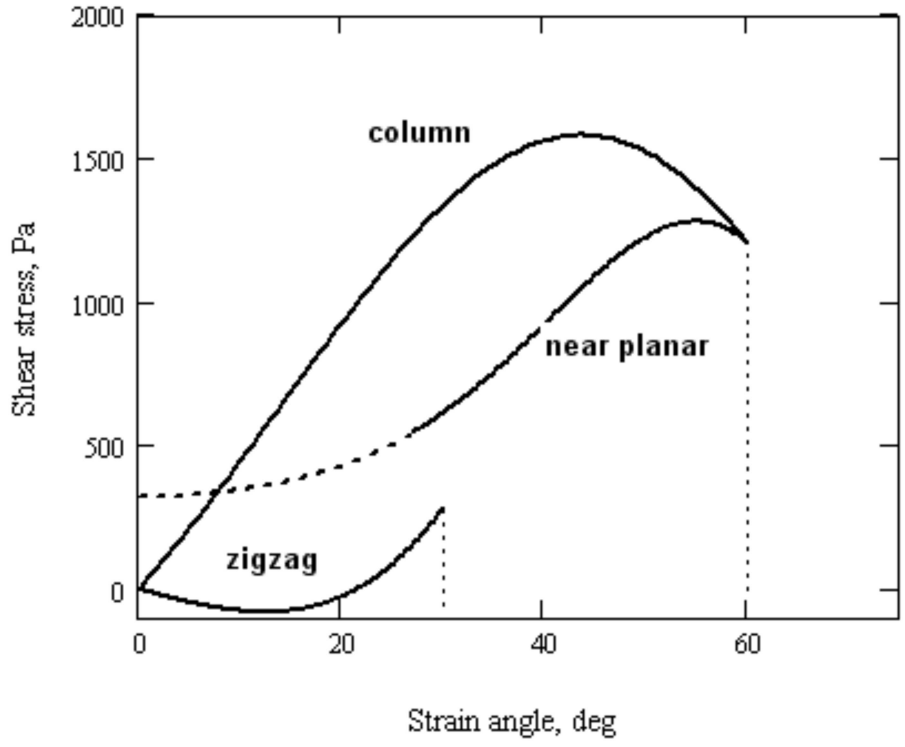
2000
1500
1000
500
0
Shear stress, Pa
column
near planar
zigzag
0
20
40
60
Strain angle, deg

Fig.9

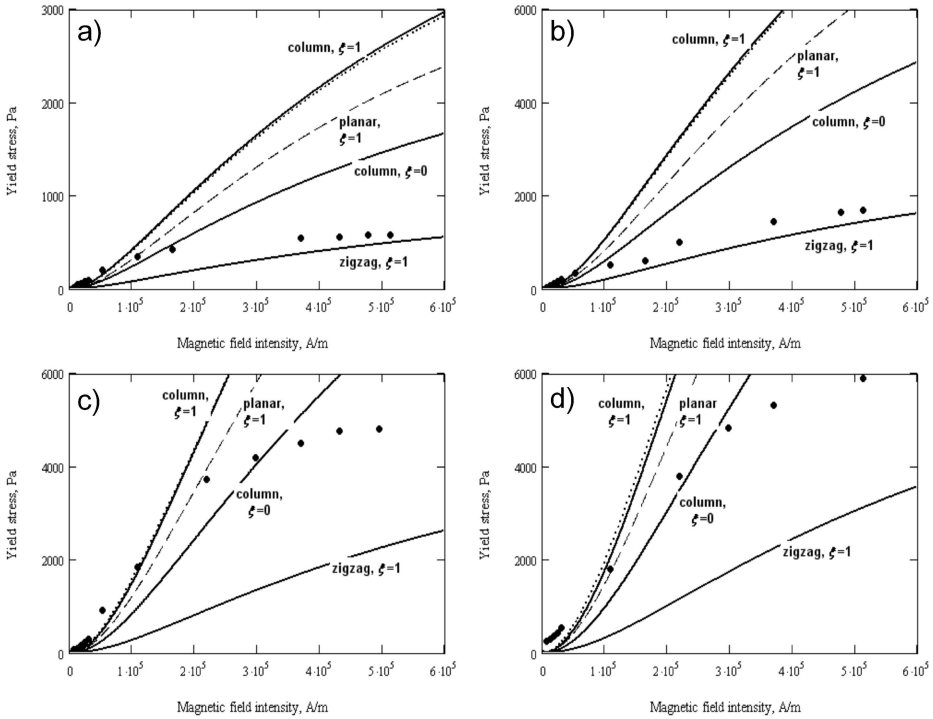
a)
column, ξ=1
planar, ξ=1
column, ξ=0
zigzag, ξ=1
b)
column, ξ=1
planar, ξ=1
column, ξ=0
zigzag, ξ=1
c)
column, ξ=1
planar, ξ=1
column, ξ=0
zigzag, ξ=1
d)
column, ξ=1
planar ξ=1
column, ξ=0
zigzag, ξ=1
Yield stress, Pa
Magnetic field intensity, A/m

Fig.10